A&A 501, 207–220 (2009)
DOI: 10.1051/0004-6361/200810715

Astronomy & Astrophysics

The Hα galaxy survey*

VII. The spatial distribution of star formation within disks and bulges

P. A. James[1], C. F. Bretherton[1,2], and J. H. Knapen[3]

[1] Astrophysics Research Institute, Liverpool John Moores University, Twelve Quays House, Egerton Wharf, Birkenhead CH41 1LD, UK
e-mail: [paj;cft]@astro.livjm.ac.uk
[2] Royal Observatory, Greenwich, London, SE10 9LF, UK
[3] Instituto de Astrofísica de Canarias, 38200 La Laguna, Spain
e-mail: jhk@.iac.es

Received 30 July 2008 / Accepted 24 April 2009

ABSTRACT

Aims. We analyse the current build-up of stellar mass within the disks and bulges of nearby galaxies through a comparison of the spatial distributions of forming and old stellar populations.
Methods. Hα and *R*-band imaging are used to determine the distributions of young and old stellar populations in 313 S0a-Im field galaxies out to ~40 Mpc. Concentration indices and mean normalised light profiles are calculated as a function of galaxy type and bar classification.
Results. The mean profiles and concentration indices show a strong and smooth dependence on galaxy type. Apart from a central deficit due to bulge/bar light in some galaxy types, mean Hα and *R*-band profiles are very similar. Mean profiles within a given type are remarkably constant even given wide ranges in galaxy luminosity and size. SBc, SBbc, and particularly SBb galaxies have profiles that are markedly different from those of unbarred galaxies. The Hα emission from individual SBb galaxies is studied in detail; virtually all show resolved central components and concentrations of star formation at or just outside the bar-end radius.
Conclusions. Galaxy type is an excellent predictor of *R*-band light profile. In field galaxies, star formation has the same radial distribution as *R*-band light, i.e. stellar mass is building at approximately constant morphology, with no strong evidence for outer truncation or inside-out disk formation. Bars have a strong impact on the radial distribution of star formation, particularly in SBb galaxies.

Key words. galaxies: spiral – galaxies: structure – galaxies: stellar content – galaxies: nuclei – galaxies: irregular

1. Introduction

Disks of spiral galaxies host the majority of the star formation activity in the local Universe (Tinsley & Danly 1980; Somerville et al. 2001; Hanish et al. 2006; James et al. 2008, henceforth Paper IV). However, there are many remaining questions regarding the formation, stability and growth of stellar disks, and the interrelation of these with other galaxy components, particularly bars and central bulge components. Star formation (SF) is shown by a wide range of indicators to be virtually ubiquitous in disks, unlike elliptical galaxies where most of the SF was completed early in their evolution. Typical current SF rates within the disks of bright, nearby spiral galaxies are 1–2 $M_\odot$ yr^{-1} (Kennicutt & Kent 1983; James et al. 2004, Paper I), sufficient to accumulate the mass of a substantial disk if continued over a Hubble time. Thus it is reasonable to ask whether the spatial distribution of new stars is consistent with that of the overall stellar mass in disks of the same type, thus motivating a picture in which disks are constructed largely through the types of SF we see at the current epoch. Alternatives are that disks could have grown from the inside outwards (Trujillo & Pohlen 2005; Muñoz-Mateos et al. 2007), resulting in the youngest stars lying on average at greater radial distances than the old stellar population; or indeed outside-in models of galaxy formation have been suggested (Gallart et al. 2008). It is also possible that spatial distributions of young and old stars could differ because of radial drifts of stellar orbits, driven by tidal torques from spiral arms, bars or external tidal interactions.

The origin of the characteristic exponential profile, found to describe the radial light distribution of many disks, has also been studied through theoretical studies (Fall & Efstathiou 1980; Freeman & Bland-Hawthorn 2002; Elmegreen et al. 2005), most of which start from the observation by Mestel (1963) that the angular momentum distribution of an exponential disk resembles that of a sphere undergoing solid-body rotation.

Observational determinations of the radial distribution of SF in galaxy disks have been performed in the past, using several approaches and observational techniques. The approaches include detailed studies of individual galaxies, e.g., Comte & Duquennoy (1982) who looked at the Sbc spiral NGC 1566, to statistical studies of typically several tens of galaxies. An early study of the latter type was carried out by Hodge & Kennicutt (1983), who considered the distributions of HII regions revealed by narrow-band Hα imaging, finding them to have characteristic ring or "doughnut" shaped distributions in early-type spirals, with more extended distributions being found in late-type

* Based on observations made with the Jacobus Kapteyn Telescope operated on the island of La Palma by the Isaac Newton Group in the Spanish Observatorio del Roque de los Muchachos of the Instituto de Astrofisica de Canarias.

spirals, and "oscillating" (non-monotonic) distributions occurring in many barred galaxies. Ryder & Dopita (1994) studied the relative scale lengths of Hα, V- and I-band emission from 34 S0–Sm galaxies, finding the line emission to have larger scale lengths than those of the continuum emission. García-Barreto et al. (1996) investigated Hα imaging of 52 barred spiral galaxies, finding nuclear rings in 10, and emission indicating SF along the bar in 18.

Dale et al. (2001) analysed Hα extents of galaxies normalised by their I-band sizes, finding no strong type dependences; similar results for Hα to R-band scalelength ratios were found by Koopmann & Kenney (2004) and Koopmann et al. (2006). Hattori et al. (2004) studied the effects of galaxy-galaxy interactions on the distributions of Hα emission within disks, finding that extended starbursts are common in such galaxies. Finally, Bendo et al. (2007) looked in detail at the SF distribution in galaxies from the SINGS sample, using 24 μm emission as the primary SF tracer. They found this emission to be typically compact and symmetric for early type galaxies, but more extended and asymmetric for late type galaxies.

The aim of this paper is to address these questions through an analysis of the spatial distribution of SF as traced by the Hα emission line in a large sample of local disk and irregular galaxies, and to compare it with the distribution of older stars. Hα provides essentially a snapshot view of SF activity, since it is powered by massive stars with main sequence lifetimes of $\sim 10^7$ years. This can cause problems with the interpretation of the Hα properties of individual galaxies, since the emission is driven by a small number of HII regions with short lifetimes, and so the stochastic uncertainties are substantial. Thus the approach adopted here is to look at the mean properties of at least several galaxies of the same type, giving a statistical basis for studies of the distribution of SF, the growth of disks, and the effects of bars on the SF process. The galaxies used are a field sample, and hence the effects of environment should be small, though some of the galaxies do have fairly close companions. These will be studied in a subsequent paper (Knapen & James 2009, Paper VIII).

All data are taken from the Hα Galaxy Survey (HαGS), a survey of 327 nearby galaxies (plus a further 7 serendipitously observed objects) which have been imaged in both the Hα line and the R-band continuum. The narrow-band filters used encompassed the Hα and neighbouring [NII] lines, which should be borne in mind when interpreting the narrow-band flux distributions in the present paper. For convenience, this combined emission is referred to as Hα throughout. The HαGS sample contains all Hubble types from S0/a to Im and galaxies are selected to have heliocentric recession velocities less than 3000 km s^{-1}. All galaxies were observed with the 1.0 m Jacobus Kapteyn Telescope (JKT), part of the Isaac Newton Group of Telescopes (ING) situated on La Palma in the Canary Islands. The selection and the observation of the sample are discussed in Paper I. The overall aim of the survey is to quantify as fully as possible the star formation properties in field galaxies at the current epoch. Earlier HαGS papers have looked at total SF rates and Hα equivalent widths in galaxies (Paper I), and the contributions of galaxies of different types to the integrated SF rate (SFR) per unit volume of the local Universe (Paper IV). Whereas previous papers derived from the HαGS have mainly focussed on integrated SF properties for each of the galaxies studied, the present paper will focus on the spatial resolution of SF provided by the Hα imaging technique. This will be done first through an analysis of three concentration indices applied to both the R-band and Hα light distributions, and then through more detailed study of mean normalised radial light distributions for galaxies of each morphological type, and for barred and unbarred galaxies.

Some results from the earlier papers that are relevant for the present study will first be summarised. Paper I contained a brief analysis of the effect of bars on total SFRs of galaxies, and on the equivalent width of Hα emission. Bars give modest, barely significant increases in both quantities overall; however, barred galaxies of types Sab–Sc inclusive were found to have larger SFRs by factors 1.5–2.0 compared with unbarred galaxies of the same types. The SFR per galaxy is highest in intermediate disk types with classifications of Sbc and Sc. In Paper IV it was found that these same types also dominate the SFR density, i.e., SFR per unit volume of the local Universe, summed over all Hubble types. Disk regions, defined as those lying more than 1 kpc from the centres of galaxies, were found to contribute more than 80% of the total SF currently occurring in the local Universe.

Sample Hα and R-band images of several galaxies from the HαGS database are presented in Paper I, and a large number of Hα images of those galaxies that have hosted supernovae are presented in the online version of another paper in this series (James & Anderson 2006, Paper III). These provide a good indication of the overall quality of the data used in the present analysis, and in the interests of brevity no images are shown in the present paper.

The structure of this paper is as follows. Section 2 contains an investigation of three concentration indices, which are applied to both Hα and R-band light distributions. The strength of correlation between indices and Hubble type is studied, leading to preliminary conclusions on the relative distributions of young and old stellar populations as a function of galaxy type. The effect of strong bars on the radial distribution of SF as traced by these indices is also analysed. Section 3 looks at mean radial profiles as a more detailed tracer of stellar distributions. Hα and R-band mean profiles, binned by type, are presented for the full sequence of spiral types, and compared for barred and unbarred types, leading to the identification of an effect on profiles for bars in SBb types that is particularly marked in Hα profiles but also clear in the R-band light distributions. The effect of continuum-subtraction errors on profiles is also studied in this section. Section 4 contains a detailed investigation of the central and bar-end Hα emission in SBb galaxies. Section 5 contains a discussion of some of the main results, and the conclusions are presented in Sect. 6.

2. Concentration indices

2.1. The concentration indices studied here

Concentration indices provide a simple measure of the observed radial distribution of the luminosity of a galaxy in a specified bandpass. They are of use since they contain much of the information contained in a galaxy classification (as will be demonstrated below) but in a quantified and less subjective form. The three indices investigated here are all measures of the "cuspiness" of the light distribution, and are sensitive to the difference between, for example, an $r^{1/4}$ law profile characteristic of an elliptical galaxy or a luminous classical bulge, where a large fraction of the light is concentrated in a central spike, and a more extended distribution such as an exponential, as would be expected for a galaxy disk. All are scale-independent, and can be applied without distance information.

The first index is the C30 index of Abraham et al. (1994) and Koopmann & Kenney (1998), which is the ratio of the flux within 0.3 times the R = 24.0 mag per square arcsec isophotal radius (henceforth r_{24}) and the total flux within that same radius.

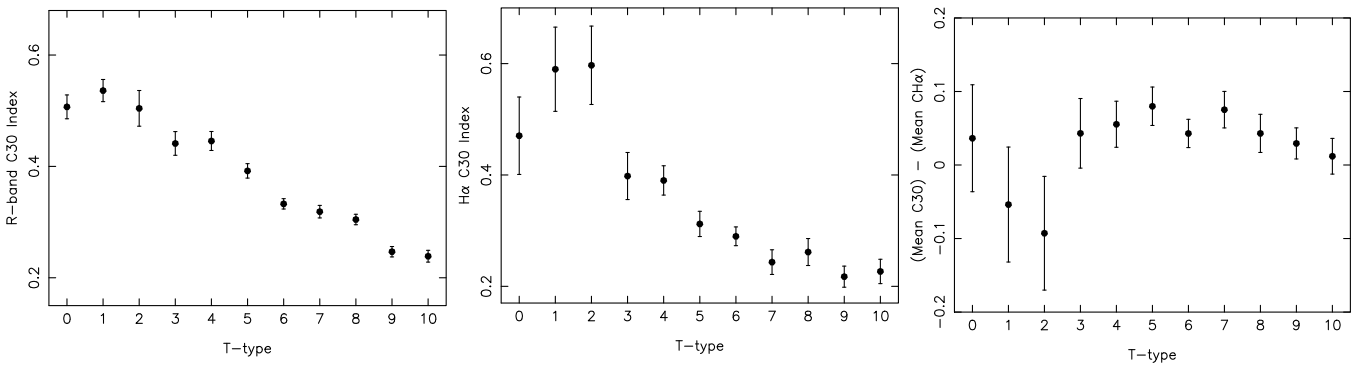

Fig. 1. The concentration index C30 plotted against Hubble type T. The plot on the left shows the mean value of the R-band C30 index for each type, with the error bars representing the standard error on the mean for all galaxies of that type. The plot in the centre shows the same mean concentration indices for Hα emission, and the plot on the right is the difference, in the sense (R-band − Hα).

Secondly, the C_{31} index (de Vaucouleurs 1977) is defined as the ratio of the radii of the apertures containing 75% and 25% of the total light, although for convenience here we use the log to the base 10 of this quantity. Other variants make use of different fractions of light, with 80% and 20% also being widely used. One drawback of C_{31} is that it requires an estimate of the total luminosity, which is generally a poorly defined quantity.

Finally, we study the Petrosian index CI_p (Shimasaku et al. 2001) which is based on the Petrosian radius (Petrosian 1976) of the galaxy under study. This is the radius at which the local surface brightness (SB) is fainter by a given factor η than the average SB within that radius. This is a useful quantity since this radius is independent of galaxy distance, K-corrections and extinction (if uniform). Here we define the Petrosian radius for an index $\eta = 0.2$; the concentration index is then the ratio of the radii containing 50% and 90% of the flux within the Petrosian radius.

In this section we investigate the correlation between these different indices and galaxy Hubble type for the HαGS sample; the sample size is sufficient for us to separate galaxies by Hubble T-type (de Vaucouleurs 1959), with the latter running from $T = 0$ (S0a) to $T = 10$ (Im). The data used are multi-aperture photometry from the CCD R-band and narrow-band continuum-subtracted Hα images from the HαGS survey. For the spiral types S0a–Sm (T-types 0–9), elliptical apertures are used, with constant ellipticity and position angle at all values of the aperture semi-major axis; these parameters are defined by galaxy isophotal shapes in the outer regions of their disks. For Im Magellanic irregulars of type $T = 10$ (and face-on spirals), circular apertures are used.

2.2. Concentration indices for R-band and Hα light as a function of galaxy type

2.2.1. The C30 index vs. type

Figure 1 shows the mean values of the C30 concentration index for R-band and Hα light (left and central plots), with the right hand plot showing the difference between the R-band and Hα mean indices. The R-band C30 index plot shows small error bars, and hence a small scatter in the index, for each Hubble T-type, both in an absolute sense and relative to the variations between T-types. This correlation of C30 with Hubble type was investigated using two methods. Firstly, a non-parametric Spearman rank analysis yields a ρ value of 0.98, well above the 99% confidence value which requires a ρ of 0.79 or greater. At the referee's suggestion, here and elsewhere we calculated an error-weighted fit assuming a linear model for the relation between these parameters. The significance of the deviations from this fit is 96% (4% probability of these residuals arising by chance). A similar correlation was also found by Koopmann & Kenney (1998, 2004) for a sample of 29 isolated galaxies of types S0–Sc (they found interestingly different results for Virgo cluster galaxies but that sample is less relevant here). Koopmann & Kenney (2004) report C30 values decreasing smoothly from 0.61–0.72 for S0 galaxies (slightly earlier than any galaxies in the present sample) to 0.24–0.37 for Sc types. Thus the range they find is very similar to that of the present study, although their Sc indices correspond more closely to those of our Sd–Im types.

The index applied to the Hα light distribution shows a substantially larger scatter, but an overall trend that is still significant according the Spearman test ($\rho = 0.94$). The significance of deviations from the best-fit linear trend is again 96%. For most types, the R-band light is more centrally concentrated in the mean than the Hα light. This is as expected given that most star formation takes place in the disks of galaxies, whereas bulges contain predominantly old stars. Types Sa and Sab are exceptions to this trend, showing marginally the opposite result. In this index, the latest types (Im; $T = 10$) show no significant difference in the mean R-band and Hα indices.

2.2.2. The C_{31} index vs. type

Secondly we investigated the mean values of C_{31} binned by galaxy type, for both R-band and Hα emission. An exponential profile has a concentration index of 0.447, whereas an $r^{1/4}$ law profile has one of 0.845. The mean concentration index variation as a function of galaxy type shows a very similar pattern to the C30 index so we omit the equivalent figure. The bulge-dominated S0/a and Sa galaxies have the highest values of R-band index, 0.64 ± 0.04, intermediate between the expectations for pure disk and pure $r^{1/4}$ bulge, as would be expected. The later type, disk-dominated, spiral galaxies and irregulars have indices $\sim 0.44 \pm 0.02$, similar to those expected for pure exponential profiles, in accordance with the findings of Kent (1985). The correlation between R-band C_{31} index and T-type is significant, with a Spearman ρ of 0.99. The significance of deviations from the best-fit linear trend is 99%.

The mean Hα C_{31} concentration index also shows a clear relationship with galaxy classification, with the late-type spirals and irregulars possessing values lower than the early types. Again, there is a larger scatter in Hα indices than for the R-band.

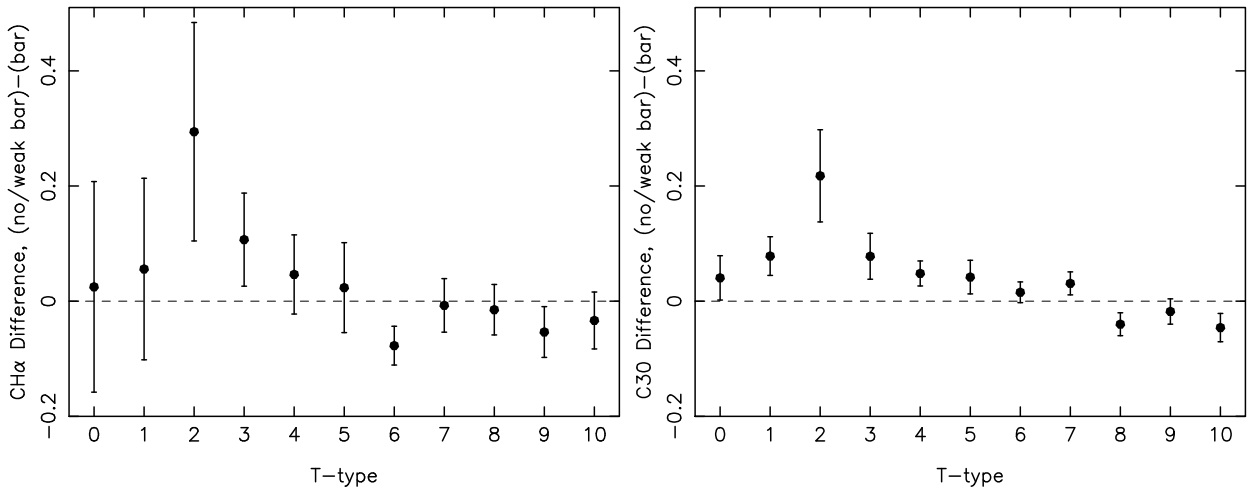

Fig. 2. The difference in mean concentration index between unbarred/weakly barred galaxies and strongly barred galaxies, plotted against Hubble type T. For points lying above the line, the unbarred/weakly barred galaxies have more centrally concentrated emission than do their strongly barred counterparts. The plot on the left shows the mean difference in this index for the Hα light distribution, and the equivalent plot for R-band continuum light is on the right.

For the later spiral types, Sc–Im, the Hα concentration index is lower than that of a pure exponential. The overall relation between Hα C_{31} index and T-type yields a Spearman ρ of 0.91 indicating high significance. The significance of deviations from the best-fit linear trend is 71%.

We also investigated the difference between R-band and Hα C_{31} indices. In most cases this difference is positive, implying that the continuum light is more centrally concentrated than the Hα. However, for this index, the higher concentration of old stars compared with star formation occurs even for the latest Hubble types, including the Magellanic irregulars, which are not thought to contain significant bulge components.

2.2.3. The Petrosian index vs. type

The Petrosian index is an inverse concentration index, so a more centrally-concentrated galaxy will have a lower value of CI_p. An exponential surface brightness profile has an index of 0.501 and an $r^{1/4}$ law profile results in a CI_p value of 0.371. Again we find the bulge-dominated S0/a and Sa galaxies to have light profiles that are close to the value expected for a pure $r^{1/4}$ law, whereas the irregulars and disk-dominated spirals have concentrations that are closer to that predicted for a pure exponential profile. The relation between R-band CI_p index and T-type is found to give a Spearman ρ of 0.98, again indicating strong correlation. The significance of deviations from the best-fit linear trend is 99.7%

A similar analysis is presented Fig. 10 in Shimasaku et al. (2001) which shows the Petrosian concentration indices for 426 SDSS galaxies against their T-type classification. The values for the HαGS galaxies appear to be systematically higher than those for the SDSS galaxies. The majority of SDSS Sa-Im galaxies have indices between 0.35 and 0.50, whereas the equivalent range for HαGS galaxies is between 0.44 and 0.57. The reasons for this offset are not clear, but it should be noted that the HαGS sample contains a large proportion of low luminosity and low surface brightness galaxies, particularly amongst the late types, which may be less fully represented in other samples.

The Hα Petrosian concentration index again has a less clean trend as a function of galaxy type than the R-band index, but the Spearman rank test still indicates a strong correlation, ρ = 0.90. The significance of deviations from the best-fit linear trend is 92%. For most types, the continuum emission appears more centrally concentrated than the Hα emission. Sab and Sb galaxies are the exception and appear to have statistically similar light distributions in R-band and Hα emission.

Overall we conclude that the C30 index seems marginally the best proxy for morphological type of the three investigated here.

2.2.4. The C30 index as an indicator of bar presence

We also carried out an analysis of the effect of bars on the mean concentration indices. Of the three indices discussed above, the C30 index was preferred for this analysis as a result of the small scatter about mean values found above for this index. Figure 2 shows the difference in the mean value of this index between unbarred or weakly barred and strongly barred galaxies (i.e., A and AB vs. B classifications). The left-hand plot shows the effect of bars on the Hα-derived index, whereas the right-hand plot is for R-band emission. The error bars show the standard error on the mean value of the difference for each type. For points lying above the line, the unbarred/weakly barred galaxies have more centrally concentrated emission than do their strongly barred counterparts. For the R-band plot, this appears to be the case for most spiral types: all the points for T = 0–7 have positive values, indicating that strong bars are associated with less centrally concentrated R-band luminosity. For the later types (T = 8–10) any effect of bars seems to be in the opposite sense, with the R-band light being somewhat more centrally concentrated than for those galaxies with no or weak bars. The relation between bar effect and galaxy T-type was investigated using the two statistical tests introduced above. The Spearman test indicates a significant correlation, with the ρ value being 0.82. The significance of deviations from the best-fit linear trend is 71%. Similar trends are seen in the left-hand plot of Fig. 2 for the distributions of Hα light. For all T-types, the scatter is larger, but again the earlier type spirals show less central concentration in the barred galaxies, with the reverse being true for later types. In this case the transition takes place between types 5 and 6 (Sc and Scd), although given the

Table 1. Number of galaxies of each Hubble T-type and bar classification contributing to the mean profiles presented in this paper.

T-type	0	1	2	3	4	5	6	7	8	9	10
A	8	6	5	5	10	16	10	9	8	24	45
AB	2	0	2	5	10	13	9	8	14	5	4
B	4	6	1	13	4	7	11	11	7	13	18
Total	14	12	8	23	24	36	30	28	29	42	67

size of the error bars the differences for any individual type are not significant. The Spearman test indicates that this correlation is significant ($\rho = 0.83$). The significance of deviations from the best-fit linear trend is 38%.

The main result from this initial analysis of barred galaxies is the lower central concentration of both old and forming stars in earlier-type barred spiral galaxies than non-barred. This effect will be studied in more detail in Sect. 4.

3. Mean light profiles in *R* and Hα light

3.1. Calculation of mean normalised light profiles

The concentration indices considered in the previous section convey only a small fraction of the information on the spatial distribution of luminosity that is contained in our images. In this section, we will present an analysis that attempts to extract more of that information, whilst still enabling meaningful averages to be taken, thus minimising the wide variations in properties that plague studies of small numbers of galaxies. This analysis makes use of normalised light profiles, which we calculate for each galaxy based on the elliptical aperture photometry that was used in the previous section to derive concentration indices. However, we choose not to present these in the form of surface brightness profiles, in units of magnitudes per square arcsec, but rather use the fluxes in the elliptical annuli, uncorrected for the increasing area of the annulus as the apertures grow. Thus the area under such a profile within a given range in radius is directly proportional to the amount of light contributed to the total luminosity of the galaxy. The shape of the resulting profile is much more intuitively related to concentration indices than is a surface brightness profile, because of this link between flux and area under the profile. For example, the effective radius can be simply estimated from such a plot as the radius which evenly divides the area under the profile.

It is necessary to normalise such profiles before combining them into, for example, a mean profile for all galaxies of a given type. A simple average without normalisation will be dominated by the brightest galaxies; and if a radial scale in kpc is adopted, then all galaxies will contribute to the centre of the mean profile, but only the largest galaxies to the outer regions, giving a distorted result that is hard to interpret. Thus we normalise the individual profiles obtained from each galaxy in two ways. Firstly, the radial scale is expressed in units of the r_{24} isophotal semi-major axis of the galaxy. Secondly, the area under each profile is normalised to unity, giving each galaxy, bright or faint, equal weighting in the mean profile. This process was applied first to the *R*-band image of each galaxy, and then to the Hα image using exactly the same positions, shapes and size of apertures, and scaling again by the *R*-band isophotal size. As a result of the normalisation, the profiles have no calibration in flux or magnitude units on the vertical axis; the profiles are simple shape functions, indicating the fraction of light residing in a given radial range.

In the remainder of this section and in the next, we look at the mean profiles produced by this process, and examine the dependence of profile shape on galaxy type, and on the presence or absence of bars. The mean profiles for the individual T-types contain between 8 and 67 profiles, as listed in Table 1, which also subdivides the numbers for each type according to bar classification. Some galaxies from the HαGS sample were omitted from this analysis due to contamination by foreground stars or problems with varying background levels across images. Hence the total number of galaxies listed in Table 1 is 313, out of the full HαGS sample of 327.

3.2. Mean profiles as a function of Hubble type

The mean profiles for all galaxies as a function of Hubble T-type are shown in Fig. 3, with the Hα profiles on the left and the *R*-band profiles on the right. The number of galaxies contributing to each profile is indicated; it is important to note that all 313 profiles of sufficient cosmetic quality have been included, so there has been no exclusion of outliers with unusual profile shapes. Error bars indicate the standard error of the individual scaled profiles about the mean at each radial point. The errors on the Hα profiles are significantly larger than those on the *R*-band profiles, originating from the clumpier nature of the Hα emission.

3.2.1. *R*-band mean profiles

The main point to note from the *R*-band profiles in Fig. 3 is the degree of correlation between mean profile shape and Hubble type, which is quite gratifying given the subjective nature of galaxy classification. The mean profiles of the earliest types (T-types 0 and 1) are very centrally concentrated, with the peak of the profiles, and hence the largest contribution to the total galaxy luminosity, coming from ~0.1 r_{24}. The one anomaly in an otherwise smooth sequence of *R*-band profiles is for the Sb galaxies ($T = 3$); the additional light in this mean profile close to the centre and at 0.4 r_{24} will be discussed in Sect. 4. For later types, the emission systematically moves outwards and broadens, with the peak sitting at ~0.4 r_{24} for the Sm and Im galaxies (T-types 9 and 10). This smooth progression in profile properties is shown in Table 2, which lists the peak and effective radii for the *R*-band and Hα mean profiles for each T-type, in units of r_{24} (the mean value of r_{24} for each type is also given in kpc in the final column, to enable approximate conversion of these values to physical units, although it should be noted that there is a large range of galaxy sizes present at each type). The same data are plotted in Fig. 4. Sizes in kpc are calculated using an effective Hubble constant of 75 km s^{-1} Mpc^{-1}, corrected for Virgo infall as explained in Paper I.

All four parameters plotted in Fig. 4 are strongly correlated with T-type, with Spearman ρ values between 0.83 and 0.95. Deviations from best-fit linear models have significances of 64–94%.

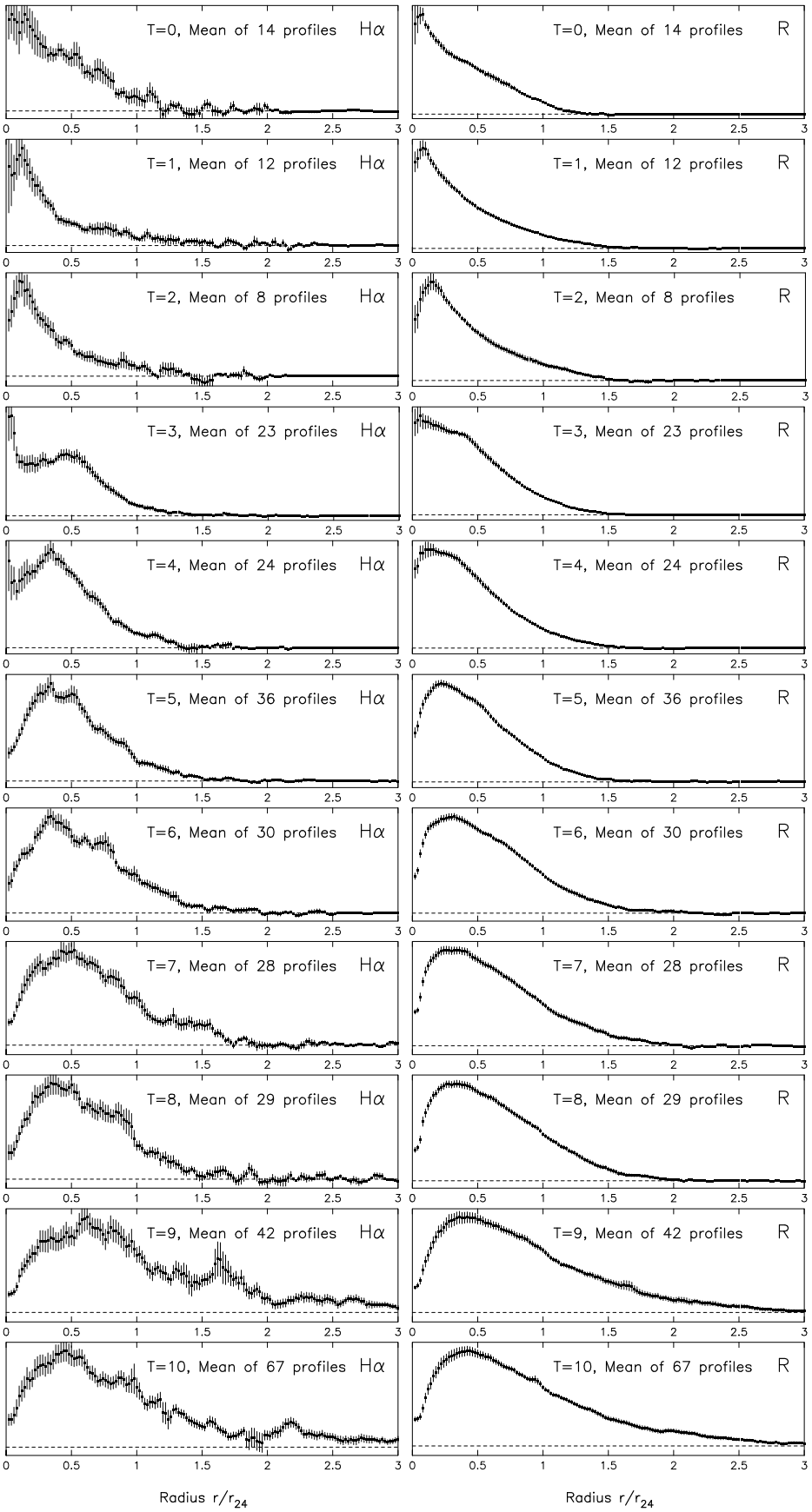

Fig. 3. Normalised mean profiles in Hα (*left*) and *R*-band light (*right*), with types from $T = 0$ to 10, *top to bottom*.

Table 2. Peak and effective radii of the Hα and *R*-band mean profiles, in units of the R_{24} isophotal radius; and the mean value of this radius, in kpc, all listed as a function of *T*-type.

T-type	Hα r_{peak}	*R* r_{peak}	Hα r_{eff}	*R* r_{eff}	$\langle r_{24} \rangle$
0	0.04	0.08	0.35	0.33	7.0
1	0.12	0.08	0.26	0.31	10.5
2	0.10	0.15	0.26	0.33	9.1
3	0.04	0.06	0.41	0.37	9.0
4	0.34	0.12	0.39	0.37	10.6
5	0.34	0.22	0.47	0.41	8.2
6	0.34	0.32	0.53	0.50	7.2
7	0.52	0.26	0.59	0.53	5.8
8	0.34	0.34	0.54	0.55	4.9
9	0.62	0.42	0.86	0.73	3.0
10	0.46	0.42	0.75	0.73	1.8

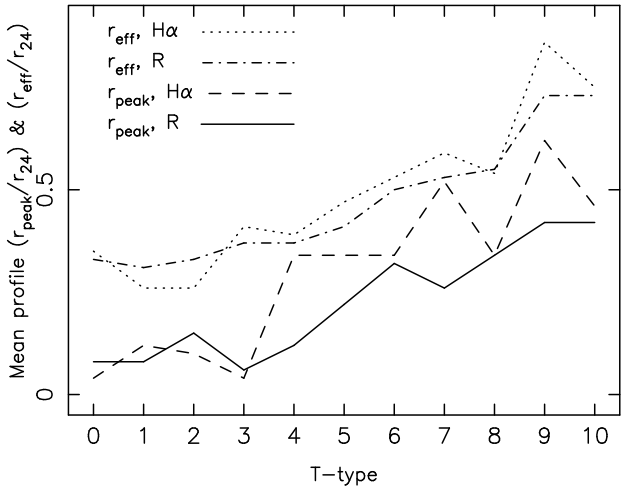

Fig. 4. Peak and effective radii of the Hα and *R*-band mean profiles, in units of the R_{24} isophotal radius.

3.2.2. Hα and (Hα – *R*) difference profiles

The mean Hα profiles are predictably less smooth than those for the *R*-band emission, but overall show a very similar trend of decreasing central concentration from early to late types. In order to emphasise any differences between the Hα and *R*-band mean profiles, we constructed difference profiles, in the sense Hα – *R*, from those shown in Fig. 3; the results are shown in Fig. 5. For the late-type spirals and Magellanic irregulars, these plots have the expected form and are simple to interpret: late-type spirals (*T* between 4 and 9 inclusive) show statistically similar distributions of *R*-band and Hα emission outside ∼0.5 r_{24}, but within this radius the relative strength Hα emission dips, presumably due to the influence of predominantly old stellar populations associated with central bulge or bar components. This "bulge dip" in the Hα emission appears to be the explanation for the lower Hα concentration indices found for *T*-types 3–9 in the right hand plot of Fig. 1.

For the Magellanic irregulars ($T = 10$), the star formation traces the *R*-band light at all radii, and there is no trace of a central older population (previously described in Paper V); this is clear evidence that these are bulge-free galaxies. It is important to note here the need to average over many tens of galaxies for this agreement to emerge. Individual Hα profiles of individual Im galaxies are very broken and spikey, since there are typically only a few HII regions per galaxy, so a statistical approach is needed to reach this conclusion. It is somewhat surprising that the central suppression of SF is clearly seen in the latest spiral types, even the $T = 9$ Sm galaxies; these might also have been thought to be "bulge-free" prior to this analysis.

The most surprising finding from Fig. 5 is that the earliest types, $T = 0$, 1 and 2, which should contain the most dominant bulges, do not show the expected central depression in their Hα – *R* profiles. For the $T = 0$ (S0a) galaxies the difference profile is consistent with being flat, within the rather large error bars, whereas the Sa and Sab profiles ($T = 1$ and 2) show emission line excesses, relative to the *R*-band light, out to radii of ∼0.3 r_{24}, which corresponds to ∼3 kpc for the average size of galaxy contributing to these profiles. The nature of such extended emission is not clear. Active Galactic Nuclei (AGN) and Low-Ionization Nuclear Emission-line Regions (LINERS) are common in galaxies of these types (Ho et al. 1997), but the line emission from such nuclei should be unresolved in our profiles. Hameed & Devereux (1999) report the finding of what they termed Extended Nuclear Emission-line Regions (ENERs) in 7 out of 27 Sa and Sab galaxies for which they had narrow-band Hα + [NII] imaging. They speculated that this emission arises from gas excited by post-Asymptotic Giant Branch stars, which would lead to the expectation that such emission should be distributed like the bulge stellar luminosity. James et al. (2005, Paper II) confirmed that central emission-line components with the same smooth morphology reported by Hameed & Devereux (1999) are present in HαGS galaxies, and demonstrated that in at least one case the emission is dominated by the [NII] line and not Hα. Such emission is qualitatively very different in appearance from the Hα emission from SF regions; the former has a smooth, diffuse and centrally symmetric structure, whereas SF regions are characteristically very clumpy and irregular. In the present sample, extended central emission regions which may be ENERs are seen in 9 out of 62 galaxies with $T = 0$ to 3, and are very rarely detected in later-type galaxies, possibly due to the dominance of the emission by that from SF. Circumnuclear rings of SF also predominantly occur in galaxies of types 3–4. They occur in up to 20% of local spiral galaxies (Knapen 2005), and at higher frequencies in types 3–4. With radii varying from a few hundred parcsec to some 2 kpc, they may also make a substantial contribution to a central peak in Hα emission in individual cases.

Outside the bulge regions, the mean Hα and *R*-band profiles of each type are essentially identical in their overall morphologies. Thus the disk SF appears to have a very similar radial distribution to the older stellar population traced by the *R*-band light. Minor differences are apparent: the Hα profiles for $T > 3$ peak at slightly larger radii than the *R*-band profiles, and the effective radii of the Hα profiles also tend to be larger (see Table 2). Both can be accounted for by the central suppression of Hα emission in bulge regions. Outside these regions, in the disk-dominated parts of the profiles, the Hα and *R*-band light distributions are identical within the errors. Thus there is no evidence of, for example, the radial truncation of Hα emission found by Koopmann & Kenney (2004) for a sample of 55 Virgo cluster spirals. This is consistent with their interpretation that the truncation is a consequence of the cluster environment (they found no truncation for a comparison sample of 29 isolated spiral galaxies), since our sample is predominantly composed of field galaxies. There is also no evidence from these profiles to support inside-out theories of disk formation; the old stellar population could have been produced by historical SF distributed like that occurring at the present epoch. The possibility of large-scale radial migration of disk material driven by, for example, bar torques obviously complicates this conclusion.

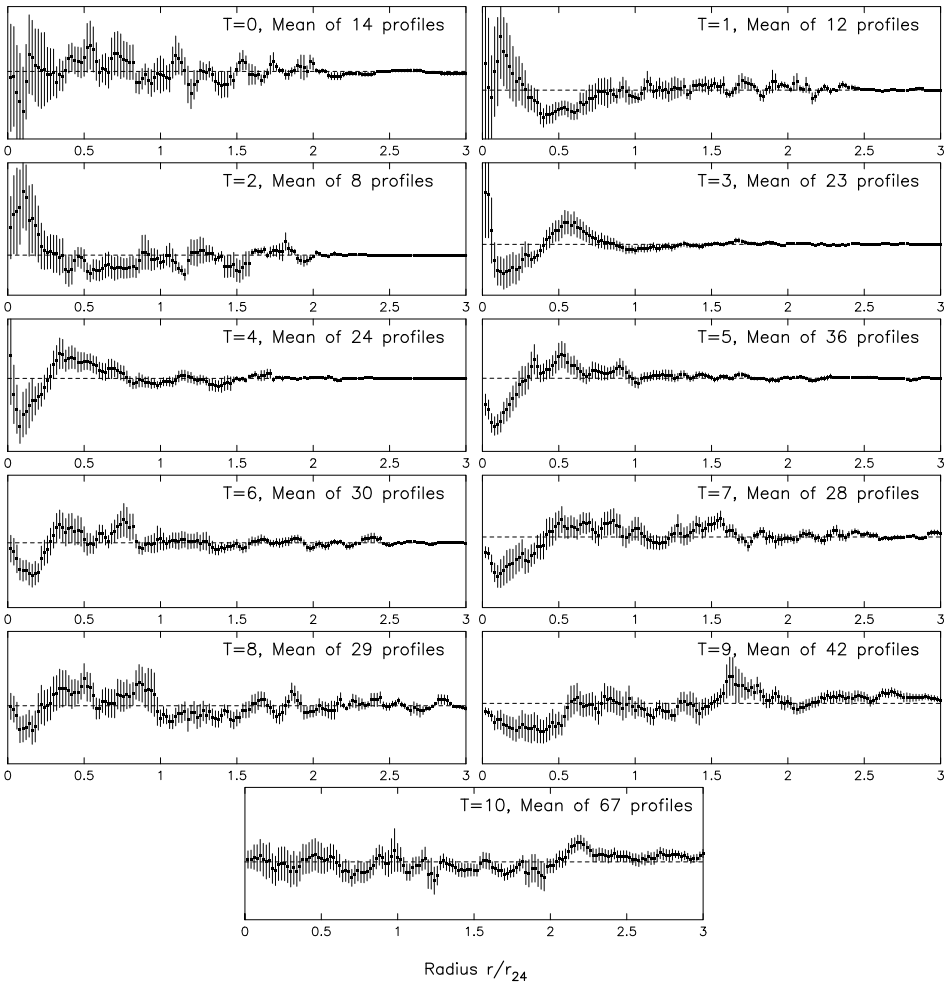

Fig. 5. Difference profiles, Hα $-R$, for all T-types.

3.2.3. The effect of continuum subtraction errors on Hα profile shape

One of the most important, and problematic, stages in the reduction of narrow-band imaging is the removal of the continuum light which passes through the narrow-band filter in addition to the desired line emission. For HαGS this was done using additional imaging through either a broad R or an intermediate-width continuum filter. The procedures and associated (significant) errors on derived total fluxes are explained in Paper I. The possibility of errors leading to under- or over-subtraction of the continuum light is particularly important for the present paper as, for example, systematic under-subtraction could easily lead to a spurious apparent agreement between the shapes of R-band and "Hα" profiles due to possible red-light contamination in the latter. A test was performed to determine the impact of continuum subtraction errors on normalised Hα profile shapes, for 10 galaxies from HαGS covering the full range of types. For each one, the scaling factor applied to the continuum image was varied by ±3 times the statistical error on this parameter, such that the residuals of unsaturated stellar images on the subtracted frame would be all negative or all positive in the two resulting frames. Thus we took conservative cases of clearly over- and under-subtracted images for this analysis. Hα profiles were then produced for each of these pairs of frames, using the methods described above.

The results of this analysis are quite reassuring. Even though continuum subtraction errors can alter total Hα fluxes by ∼30%, the effects on the shapes of profiles, after renormalising the profile area to unity, is much smaller. Figure 6 shows, for a selection of the 10 galaxies studied, that the strongest effects are unsurprisingly found in the central regions of early-type galaxies, since these are dominated by high surface brightness bulges. However, even in these cases the overall shapes of the derived Hα profiles are not greatly affected. The Hα effective radii for UGC 4097 and UGC 4273, which show the greatest variation in profile shape in Fig. 6, both change by ±2.5% as a result of this degree of continuum over- and under-subtraction. For galaxies of type Sc or later, the effects of continuum subtraction errors on profile shape are negligible.

3.2.4. Dependence of profiles on galaxy distance, size and luminosity

The strong dependence of R-band profile shape on T type, and the generally small error bars on the R-band profile points in Fig. 3, indicate a high degree of uniformity of light profiles which is somewhat surprising given the range of properties of the galaxies contributing to each profile. The 36 galaxies contributing to the $T = 5$ profiles lie at distances ranging from 2.1 to 34 Mpc, and have R-band absolute mags from –16.1 to –21.6, corresponding to a factor of 160 in luminosity; for the 42

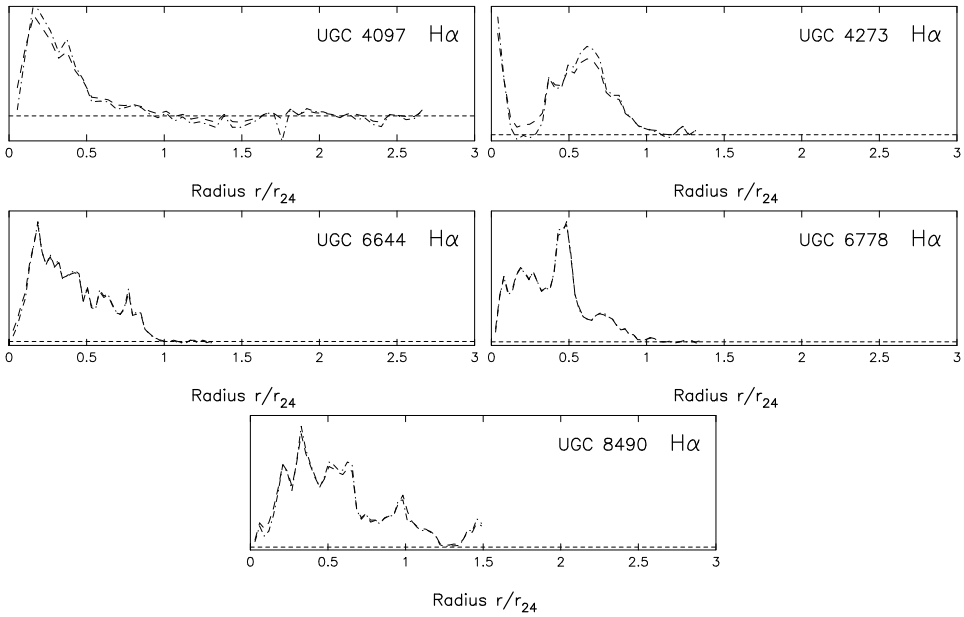

Fig. 6. Profiles made with the continuum light deliberately over- and under-subtracted (dot-dashed and dashed curves respectively), for five representative sample galaxies: UGC 4097 (Sa), UGC 4273 (SBb), UGC 6644 (Sc), UGC 6778 (SABc) and UGC 8490 (Sm).

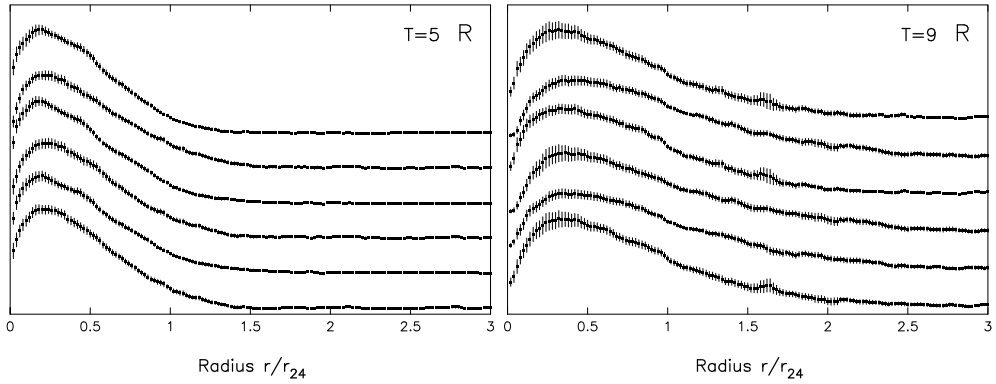

Fig. 7. Mean *R*-band light profiles for $T = 5$ galaxies (*left*) and $T = 9$ galaxies (*right*), with the 6 profiles in each frame showing the bright, faint, large, small, far and near halves of the total sample from top to bottom.

$T = 9$ galaxies, the distance range is similar, and the luminosity range still larger at a factor of 360 (M_R from –12.9 to –19.3). We have thus checked for any dependence of the mean profile shape on distance, galaxy radius in kpc, and luminosity, using these two types as test cases due to the large numbers of profiles available and the large range of properties included in each type. The results are shown in Fig. 7. Each panel shows the mean *R*-band profiles for one half of the galaxies of the appropriate type, with the split being done by distance, galaxy radius and *R*-band luminosity. $T = 5$ galaxy profiles are on the left, those for $T = 9$ on the right. For $T = 5$, the only effects seen are the appearance of a subtle "shoulder" at 0.5 r_{24} in the bright, large and distant halves of the sample, but the overall shapes of the profiles are all very similar. For $T = 9$, the bright and large halves of the sample have mean profiles that are somewhat more centrally concentrated than the faint half. The bright half matches the overall $T = 8$ profile in peak position (0.34 r_{24}), and has an effective radius (0.64 r_{24}) between those for the $T = 8$ and $T = 9$ profiles. Thus the luminosity dependence appears slight, and overall we conclude that profile shape is largely determined by galaxy classification.

4. The effects of bars on distributions of star formation and continuum light

4.1. Mean light profiles for barred and unbarred galaxies

The mean *R*-band profile for Sb galaxies ($T = 3$) in Fig. 3 shows a distinctive "shoulder" on the central emission peak, extending to a radius of ∼0.5 r_{24}. The same effect is seen, albeit less strongly, in the mean Sbc profile. The mean Hα profiles of these two types are also distinctive, with a narrow central peak, a *minimum* in the profile (not seen for any other types), and an outer maximum which is at an anomalously large radius given the relatively early types (see Table 2). This is particularly marked for the Sb mean profile. The size corresponding to the "shoulder" radius for the Sb profile is 4.8 kpc, which immediately suggests that the excess light may be due to bars. Indeed, 13 of the 23 galaxies contributing to this mean profile are classified SBb. To investigate this possibility, in Figs. 8 and 9 we have replotted the Hα and *R*-band mean light profiles of Fig. 3 subdivided according to bar type. In each figure, the left-hand plots show mean profiles for galaxies classified as showing no evidence for

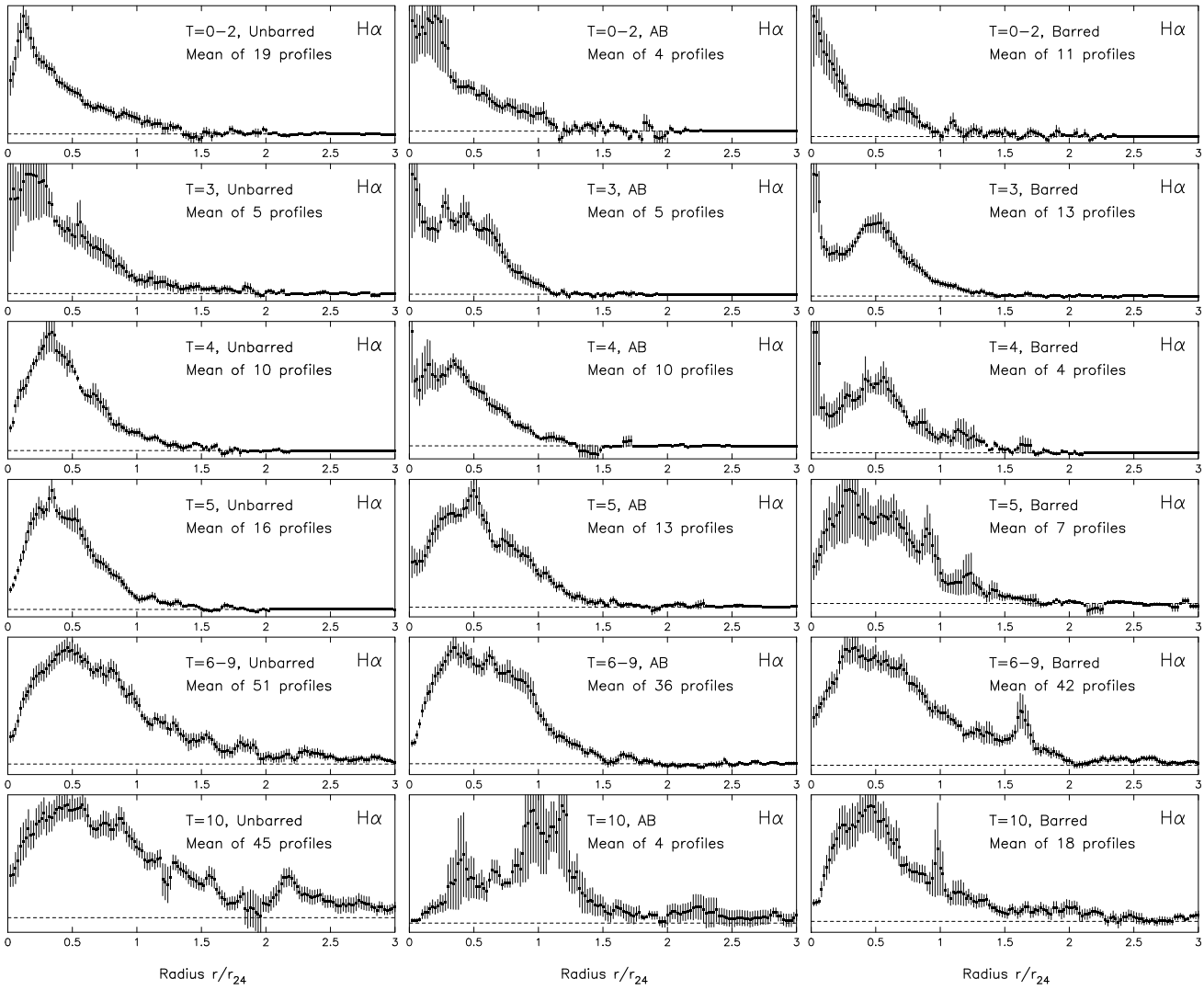

Fig. 8. Mean Hα light profiles, as shown in Fig. 3, but subdivided into unbarred, AB and barred galaxies, in left, middle and right frames respectively.

bars in their optical morphologies (St/SAt, or Im); the central plots show those for intermediate or possible bar types (SABt or IABm); and the right-hand plots the profiles for galaxies with clear optical bars (SBt or IBm). Bar classifications are taken from de Vaucouleurs et al. (1991) who used optical images; it should be noted that near-IR imaging can reveal weak or small bars not seen in the optical. In order to maintain reasonable numbers in each mean profile, early (T = 0–2) and late (T = 6–9) spiral types have been combined. Types 3–5 are plotted separately as these are the most important for the following discussion.

Figures 8 and 9 confirm that the distinctive profiles seen for the T = 3 galaxies are indeed due to the barred SBb galaxies. The mean Hα profile for the SBb galaxies shows a very strong central peak of emission, and a clear outer peak at 0.5 r_{24}. Both are absent in the mean profile of the Sb (unbarred) galaxies, and indeed from the mean profiles of the unbarred galaxies of any T type. The profile for the T = 3 SABb galaxies is noisy, given that only 5 galaxies contribute, but appears intermediate between those of the Sb and SBb types, with some evidence of a central peak. The R-band mean profiles for Sb, SABb and SBb types show the same pattern, with the characteristic bar features being somewhat less strong in the older stellar population. The SBb R-band profile still has a central peak, and an outer peak at 0.5 r_{24}, but both represent a much smaller fraction of the overall flux than is the case for the mean Hα profile. Bars thus have a substantial effect on the R-band light distribution for T = 3 galaxies, with the outer peak pushing a large fraction of the flux further out in these galaxies, an effect which explains the lower concentration indices for barred galaxies illustrated in Fig. 2. Indeed, the effect on the concentration indices would presumably be even more marked were it not for the central peaks in the mean barred profiles, which must act to increase the concentration indices.

These characteristic bar profiles occur for T = 3 galaxies where they are most apparent, but also for T = 4 galaxies, and possibly for those of T = 5. (In comparing the T = 3 and 4 barred mean profiles, it should be noted that there are 13 SBb galaxies contributing to the mean profiles against only 4 of type SBbc, so inevitably the mean profile for the latter type is more noisy.) The mean Hα profile for the SBbc (T = 4) galaxies is clearly different from that for the SBc (T = 5) galaxies, with the former again having a central peak and an outer peak at ~0.5r_{24}, like those in the SBb mean profile. The SBbc R-band profile shows only a weak central peak, and the outer profile shows a "shoulder" of flux pushed to larger radius, but no outer peak as such. For T = 5, the only effect is the broadening of the mean profiles, with flux again pushed to larger radii. The Hα profile is

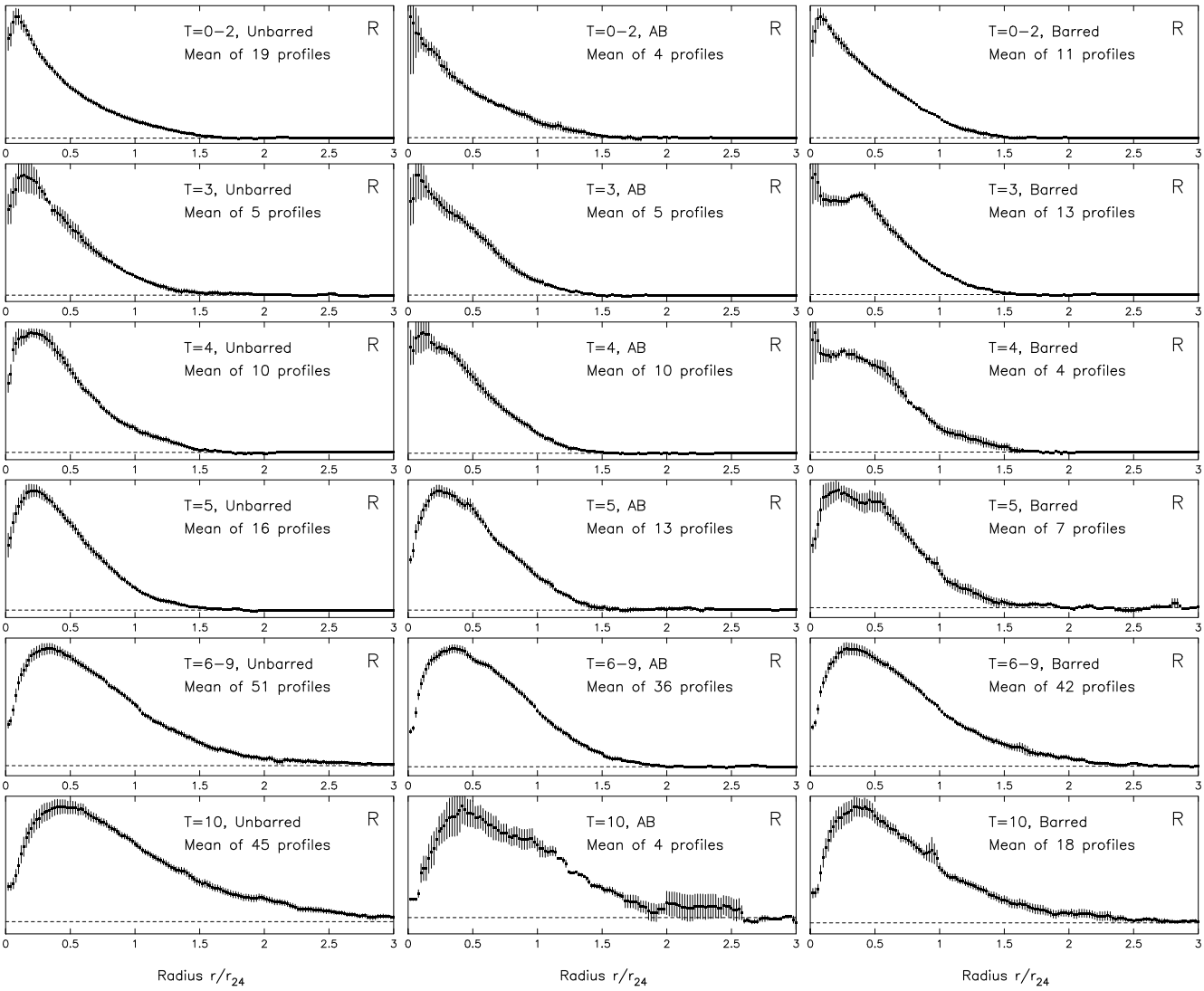

Fig. 9. As Fig. 8 but showing the *R*-band profiles, again subdivided by bar classification.

noisy at all radii, but the *R*-band profile shows evidence for this additional flux causing a "shoulder" in the profile. No central or outer peaks are seen in the $T = 5$ mean profiles, or indeed in any of the profiles for types later than this.

Thus we have identified a clear effect of bars on the pattern of SF as a function of radius within galaxy disks, which results in strongly enhanced Hα emission, and moderately enhanced *R*-band emission, in both the central regions and at 0.5 r_{24}. This effect seems to apply most strongly to those galaxies classified as SBb or SBbc ($T = 3, 4$), where the overall distributions of SF are profoundly different from their unbarred counterparts. It should be recalled that the mean profiles we show here are constructed such that areas under the profiles are directly proportional to fractions of total flux. Thus inspection of the SBb mean Hα profile shows that a significant fraction of the total Hα + [NII] emission from these galaxies is associated with the outer peak feature.

The greater strength of the bar-induced features in the Hα mean profiles than in the *R*-band profiles is important, since this confirms that the bars are inducing SF that would not otherwise be happening, and are not merely redistributing pre-existing stellar populations. If the latter were the case, the amplitude of the effect would be the same in *R*-band light and Hα (see Seigar & James 2002, for a similar argument applied to the triggering of SF by spiral arms).

Having identified this characteristic pattern of SF in SBb galaxies, we next investigate the nature of both nuclear and outer emission peaks, by looking in detail at the continuum-subtracted Hα images for all galaxies of this type in the HαGS sample.

4.2. Individual SBb galaxies: nuclear emission peaks

To study in more detail the origin of the central peak in Hα in SBb ($T = 3$) galaxies and, in the next subsection, that of the peak near 0.5 r_{24}, we consider here the properties of the 14 individual galaxies that make up this subsample. The properties of the central emission-line peaks seen in these 14 galaxies are listed in Table 3 (UGC 6123, which was omitted from the mean profiles because of a bright superposed star, is reinstated in this table; note that this galaxy does show both nuclear and bar-end emission). The major conclusion to draw from Table 3 is the near-ubiquity of nuclear peaks, which are found in 13 of the 14 SBb galaxies (denoted by "Y" in Col. 5).

Table 3. Properties of the central emission peaks.

UGC	NGC	Classn.	Dist. Mpc	Peak	Res	*FWHM* kpc
3685	–	SB(rs)b	26	Y	U	<0.17
4273	2543	SB(s)b	35	Y	R	0.65
4484	2608	SB(s)b	32	Y	R	0.34
4574	2633	SB(s)b	31	Y	R	0.62
4705[1]	2710	SB(rs)b	36	Y	R+	1.10
4708	2712	SB(r)b:	29	Y	R+	1.20
6077	3485	SB(r)b:	27	Y	R	0.29
6123[2]	3507	SB(s)b	21	Y	R?	–
6595[3]	3769	SB(r)b:	12	Y	R+	0.32
7002	4037	SB(rs)b:	18	Y	R?	0.24
7523[4]	4394	(R)SB(r)b:	18	Y	R+	0.46
7753[5]	4548	SB(rs)b	18	Y	R+	0.45
9649[6]	5832	SB(rs)b?	8	N	–	–
12699[7]	7714	SB(s)b:p	31	Y	R?	0.32

[1] Emission elongated along bar axis. [2] LINER; foreground star contamination, so not in mean profiles. [3] Interacting with NGC 3769A, type Sm. [4] LINER; Smooth extended emission, possible ENER. [5] M91; LINER/Seyfert; possible ENER. [6] Classified as SBc in UGC. [7] HII/LINER; tidally distorted.
For each galaxy, we list the UGC and NGC catalogue numbers, the full galaxy classifications from de Vaucouleurs et al. (1991), the distance in Mpc from Paper I, whether or not the galaxy exhibits a central peak in Hα emission, the resolution of the peak as explained in Sect. 4.2, and the FWHM of the emission, in kpc. All LINER/Seyfert classifications in the footnotes are taken from the NASA/IPAC Extragalactic Database (NED).

Table 4. Properties of the outer emission peaks.

UGC	NGC	Classn.	Peak	r r_{24}	r kpc	Morph
3685	–	SB(rs)b	Y	0.58	4.5	RB[1]
4273	2543	SB(s)b	Y	0.60	8.3	BE2
4484	2608	SB(s)b	Y	0.56	5.8	BE2
4574	2633	SB(s)b	Y	0.40	5.2	BE2
4705	2710	SB(rs)b	Y	0.46	4.8	RB[1]
4708	2712	SB(r)b:	Y	0.36	4.4	BE1
6077	3485	SB(r)b:	Y	0.54	4.0	RB[1]
6123	3507	SB(s)b	Y	–	–	BE1[2]
6595	3769	SB(r)b:	N	–	–	–
7002	4037	SB(rs)b:	Y	0.54	3.1	BE1
7523	4394	(R)SB(r)b:	Y	0.44	3.6	R[1]
7753	4548	SB(rs)b	Y	0.48	6.4	BE2
9649	5832	SB(rs)b?	Y	0.54	1.7	BE2
12699	7714	SB(s)b:p	N	–	–	–

[1] Ring at same radius as bar ends. [2] SF at one bar end; other behind foreground star.
Columns 1 to 3 are as in Table 3, and the remaining entries denote whether the galaxy exhibits an outer peak in the Hα profile, give the radius of the peak centre in units of the r_{24} radius and in kpc, and finally describe the morphology of the peak, as explained in Sect. 4.3.

Table 3 also contains information on the sizes of the central peaks. That for UGC 3685 is unusual in that it is unresolved in our Hα image ("U" in the Col. 6), i.e. the FWHM of the peak is consistent with that of stellar images in the same image before continuum subtraction. This favours an AGN interpretation for this emission, as a typical SF complex would be resolved at the distance of this galaxy. All the other central profiles are marginally resolved ("R?") or resolved ("R"; "R+" implies the source is several times larger than the seeing disk). The approximate diameter of the emission line region is given in Col. 7. For the resolved regions this is typically a few hundred pc, which would imply the presence of SF complexes or nuclear rings of SF. However, this does not exclude the possibility of AGN emission in many or all of these galaxies, and indeed four of those with extended emission are known to have LINER-type nuclei. In two of these (UGC 7523 = NGC 4394 and UGC 7753 = M 91) the extended emission has the smooth morphology characteristic of ENERs.

Two of the galaxies in Table 3 will be discussed in more detail in Paper VIII; these are the luminous interacting galaxy NGC 7714, and NGC 3769.

4.3. Individual SBb galaxies: outer emission peaks

The properties of the regions contributing to the line emission at a radius of ~0.5 r_{24} are summarised in Table 4. Here the fourth column indicates whether the individual Hα profile for the galaxy concerned exhibits such an outer peak, Cols. 5 and 6 give the radius of the peak in units of the r_{24} radius and kpc respectively; and the final column contains descriptors of the morphology of the emission-line regions leading to this peak, obtained through inspection of the continuum-subtracted Hα images. "R" denotes a ring morphology, "RB" a broken or partial ring, "BE1" emission predominantly from one end of the bar, and "BE2" emission from both bar ends.

In this case we find that 11 of the 13 galaxies contributing to the mean SBb profile have clear outer peaks in their mean light profiles. The contaminated image of UGC 6123 shows emission from the one end of the bar that is clearly visible, but the foreground star makes it impossible to decide between "BE1" and "BE2" designations for this galaxy.

5. Discussion

5.1. Concentration indices

Three different concentration indices have been investigated in Sect. 2. All three methods show a strong correlation with Hubble type, with the early-type, bulge-dominated galaxies having concentration indices close to those expected for an $r^{1/4}$ profile and the late types approximating to those of exponential profiles. Investigation of the relative concentrations finds that most galaxies are more centrally concentrated in the continuum light than in the Hα. Strong bars tend to decrease the central concentration of R-band light, and to a smaller extent the Hα light, over most disk types. For the latest type barred galaxies (SBdm–IBm) the reverse trend is seen.

5.2. Radial profiles

From our radial flux profiles, we identify two features that are seen in barred galaxies of morphological types $T = 3$ and 4 but not in un-barred galaxies of those types, which are a central peak of emission and a second peak at 0.5 r_{24}. As was was discussed in Sect. 4.2, the nuclear peak is most probably due to nuclear emission not related to SF, ENERs, and/or circumnuclear rings. The second peak occurs just outside the end of the bar, and may be related to the presence of an inner (pseudo-ring) as known to exist in many galaxies.

From the mean Hα profile, we can estimate the overall importance of the SF related to these features. We find that ~50% of the current massive SF activity in type $T = 3$ and 4 galaxies

occurs in the radial range of the outer peak. The *excess* SF is somewhat harder to estimate, but flattening the "hump" between 0.26 and 0.72 r_{24} reduces the overall SFR by ∼20%. This implies that inner (pseudo)-rings or other features at the radial position of the end of the bar contain a significant fraction of the total massive SF activity in the galaxies under consideration. The equivalent number for the central peak is ∼10%.

We thus confirm that barred galaxies of T-types 3 and 4 have strong concentrations of SF both in their central regions (with the caveat that some part of the emission we base this statement on may be due to non-stellar processes) and in the regions at the ends of the bar.

5.3. Inner rings

The galaxy classifications in the Col. 3 of Table 4 show that four have an "(r)" classification, indicating an inner ring, and five "(rs)" indicating a pseudo-ring. This frequency is similar to or slightly higher than the fraction expected from the numbers of such rings found in $T = 3$ galaxies by Buta & Combes (1996). The radial size of the outer peaks found in the present study is similar to that of inner rings, but the match is not perfect. de Vaucouleurs & Buta (1980) give a formula for the radial size of inner rings as a function of galaxy type and bar classification. For SBb galaxies, this formula predicts inner rings to have radii 0.303 times the B_{25} isophotal radius, where the latter is very similar to the R_{24} isophotal radius used in the present study. The R-band outer peaks are centred on 0.38 times the R_{24} isophotal radius, ∼25% larger than is expected for inner rings; and the Hα outer peaks are at somewhat larger radii still, 0.4–0.5 times this isophotal radius. This implies that the SF we are seeing is not directly associated with the bar ends, but is triggered in the spiral arms lying just beyond this radius. In this context, it should be noted that NGC 4548, one of the SBb galaxies in the present study, is the prototype for the "bracket type" of barred galaxies (Buta et al. 2002), where short spiral arms lie just outside the radius of the bar ends, and "overshoot" the bar, rather than starting where the bar terminates. In this galaxy at least, the SF causing the outer peak is clearly located in these arm segments.

5.4. Bars and star formation

The impact of the presence of a bar on the total SFR in a galaxy has been studied by many authors (e.g., Hawarden et al. 1986; Dressel 1988; Puxley et al. 1988; Pompea & Rieke 1990; Isobe & Feigelson 1992; Ryder & Dopita 1994; Tomita et al. 1996; Huang et al. 1996; Martinet & Friedli 1997; Aguerri 1999; Sheth et al. 2002; Roussel et al. 2001; Verley et al. 2007), but no consensus has been reached as to whether the presence of bars causes a global enhancement of the SFR.

One of the most important characteristics of bars is that the non-axisymmetric mass distribution in their host galaxy can lead to the outward transport of angular momentum, and thus to the inward transport of gas (see, e.g., the review of Shlosman et al. 1990, for the theoretical view). The resulting enhanced central concentration of gas in barred galaxies as compared to non-barred galaxies has indeed been observed (e.g., Sakamoto et al. 1999; Sheth et al. 2005), although Komugi et al. (2008) note that varying Hubble type, indicative of the effect of the bulge, is more important for central gas concentration than the presence of a bar.

The central gas concentration caused by bars may lead to an enhanced SFR rate in bars, quite possibly in the form of circumnuclear rings of SF which can occur between the inner Lindblad resonances set up by the bar. Indeed, almost all of these nuclear rings occur in barred galaxies, and in the few that do not the influence of a past interaction can often be deduced (e.g., Knapen 2005). Whether nuclear starburst and AGN activity is, statistically, induced or facilitated by the presence of a bar is not a settled question, with theoretical studies supporting such a link (Shlosman et al. 1989; Wada & Habe 1995; Wada 2004; Shlosman et al. 2000), whilst observations have hinted both in favour of (Knapen et al. 2000; Laine et al. 2002; Hunt & Malkan 2004) and against (Mulchaey & Regan 1997; Martini et al. 2003; Laurikainen et al. 2004; Dumas et al. 2007) this connection. A review by Knapen (2004) concludes that the evidence favours a slight effect connecting bars to both these types of activity, but the link is statistical and not direct, and subject to important caveats.

What has been studied perhaps less in the literature is what we present here: an analysis of the effect on bars on the radial distribution of current and past SF in disk galaxies. In addition, all past studies have considered radial profiles in surface brightness or equivalent, rather than the kind of flux profiles we present here, and which show much more clearly the effects of different components on the radial profiles. The classical study of observed bar properties, including radial surface brightness profiles, is that by Elmegreen & Elmegreen (1985), although before that other papers, such as those by de Vaucouleurs & Freeman (1972) and Elmegreen & Elmegreen (1980) had considered the Large Magellanic Cloud (LMC) and other late-type galaxies that resemble it. A common finding in all these, and subsequent, papers is that important areas of massive SF appear near the ends of the bar.

6. Conclusions

The spatial distributions of Hα and R-band light have been investigated for a sample of 313 nearby S0a–Im galaxies. The initial analysis employed three concentration indices, all of which showed declining central concentration of light in both bandpasses as a function of increasing T-type; somewhat lower concentration in Hα than R-band for most T-types; and a moderate decrease in the central concentration of luminosity for barred cf. unbarred galaxies for $T = 0$–5 early to intermediate spiral types. Mean normalised profiles were then introduced as a more detailed probe of light distributions in the two bandpasses. These profiles show a smooth sequence in properties as a function of galaxy type, with a hump containing most of the flux shifting to larger values of the normalised radius as T increases. The profiles at a given T-type were found to show a remarkably small scatter from galaxy to galaxy; this was investigated at R for the two spiral types with the largest number of individual profiles, and profile shape was found to show no significant dependence on galaxy size, luminosity or distance.

The central regions of the Hα profiles of most galaxy types were found to show a dip relative to the R-band profiles, which we interpret as the signature of the older stellar populations in bulges and bars, cf. disks. Surprisingly, this central dip is not present in the mean light profiles of the earliest types studied here ($T = 0$–2), probably due to a combination of nuclear SF rings and non-SF-related ENER emission in the central regions of many of these galaxies. The mean Hα and R-band profiles of the latest types (particularly $T = 10$ Im types) show excellent agreement in overall shape. There is no evidence for outer

truncation of the mean Hα profiles relative to the R-band profiles for any type.

The mean Hα profile for SAb, SABb and SBb ($T = 3$) galaxies showed a central spike, and an outer peak at ~0.45 r_{24}. Both were found to be characteristic features of barred $T = 3$ galaxies, occurring in almost all of the individual galaxies of this type, and were present at a lower level in the R-band mean $T = 3$ profile, and in the mean profiles for galaxies of T-types 4 and 5. The outer peaks are at radii similar to or somewhat larger than those expected for inner rings, and they constitute at least 20% of the total SF activity in the SBb galaxies. The central spikes are resolved in most cases, implying that they are not purely powered by AGN activity, and contribute ~10% of the total Hα flux.

Acknowledgements. The Jacobus Kapteyn Telescope was operated on the island of La Palma by the Isaac Newton Group in the Spanish Observatorio del Roque de los Muchachos of the Instituto de Astrofísica de Canarias. This research has made use of the NASA/IPAC Extragalactic Database (NED) which is operated by the Jet Propulsion Laboratory, California Institute of Technology, under contract with the National Aeronautics and Space Administration.

References

Abraham, R. G., Valdes, F., Yee, H. K. C., & van den Bergh, S. 1994, ApJ, 432, 75
Aguerri, J. A. L. 1999, A&A, 351, 43
Bendo, G. J., Calzetti, D., Engelbracht, C. W., et al. 2007, MNRAS, 380, 1313
Buta, R., & Combes, F. 1996, Fund. Cosmic Phys., 17, 95
Buta, R., Corwin, Jr., H. G., & Odewahn, S. C. 2002, in Disks of Galaxies: Kinematics, Dynamics and Peturbations, ed. E. Athanassoula, A. Bosma, & R. Mujica, ASP Conf. Ser., 275, 102
Comte, G., & Duquennoy, A. 1982, A&A, 114, 7
Dale, D. A., Giovanelli, R., Haynes, M. P., Hardy, E., & Campusano, L. E. 2001, AJ, 121, 1886
de Vaucouleurs, G. 1959, Handbuch Phys., 53, 275
de Vaucouleurs, G., & Freeman, K. C. 1972, Vistas Astron., 14, 163
de Vaucouleurs, G. 1977, in Evolution of Galaxies and Stellar Populations, ed. B. M. Tinsley, & R. B. Larson, 43
de Vaucouleurs, G., & Buta, R. 1980, ApJS, 44, 451
de Vaucouleurs, G., de Vaucouleurs, A., Corwin, Jr., H. G., et al. 1991, Third Reference Catalogue of Bright Galaxies, Vol. 1–3, XII (Berlin, Heidelberg, New York: Springer-Verlag), 2069
Dressel, L. L. 1988, ApJ, 329, L69
Dumas, G., Mundell, C. G., Emsellem, E., & Nagar, N. M. 2007, MNRAS, 379, 1249
Elmegreen, B. G., & Elmegreen, D. M. 1985, ApJ, 288, 438
Elmegreen, B. G., Elmegreen, D. M., Vollbach, D. R., Foster, E. R., & Ferguson, T. E. 2005, ApJ, 634, 101
Elmegreen, D. M., & Elmegreen, B. G. 1980, AJ, 85, 1325
Fall, S. M., & Efstathiou, G. 1980, MNRAS, 193, 189
Freeman, K., & Bland-Hawthorn, J. 2002, ARA&A, 40, 487
Gallart, C., Stetson, P. B., Meschin, I. P., Pont, F., & Hardy, E. 2008, ApJ, 682, L89
García-Barreto, J. A., Franco, J., Carrillo, R., Venegas, S., & Escalante-Ramírez, B. 1996, Rev. Mex. Astron. Astrofis., 32, 89
Hameed, S., & Devereux, N. 1999, AJ, 118, 730
Hanish, D. J., Meurer, G. R., Ferguson, H. C., et al. 2006, ApJ, 649, 150
Hattori, T., Yoshida, M., Ohtani, H., et al. 2004, AJ, 127, 736
Hawarden, T. G., Mountain, C. M., Leggett, S. K., & Puxley, P. J. 1986, MNRAS, 221, 41P
Ho, L. C., Filippenko, A. V., & Sargent, W. L. W. 1997, ApJ, 487, 568
Hodge, P. W., & Kennicutt, Jr., R. C. 1983, ApJ, 267, 563
Huang, J. H., Gu, Q. S., Su, H. J., et al. 1996, A&A, 313, 13
Hunt, L. K., & Malkan, M. A. 2004, ApJ, 616, 707
Isobe, T., & Feigelson, E. D. 1992, ApJS, 79, 197
James, P. A., & Anderson, J. P. 2006, A&A, 453, 57 (Paper III)
James, P. A., Shane, N. S., Beckman, J. E., et al. 2004, A&A, 414, 23 (Paper I)
James, P. A., Shane, N. S., Knapen, J. H., Etherton, J., & Percival, S. M. 2005, A&A, 429, 851 (Paper II)
James, P. A., Knapen, J. H., Shane, N. S., Baldry, I. K., & de Jong, R. S. 2008, A&A, 482, 507 (Paper IV)
Kennicutt, Jr., R. C., & Kent, S. M. 1983, AJ, 88, 1094
Kent, S. M. 1985, ApJS, 59, 115
Knapen, J. 2004, in The Neutral ISM in Starburst Galaxies, ed. S. Aalto, S. Huttemeister, & A. Pedlar, ASP Conf. Ser., 320, 205
Knapen, J. H. 2005, A&A, 429, 141
Knapen, J. H., & James, P. A. 2009, ApJ, 698, 1437 (Paper VIII)
Knapen, J. H., Shlosman, I., & Peletier, R. F. 2000, ApJ, 529, 93
Komugi, S., Sofue, Y., Kohno, K., et al. 2008, ArXiv e-prints, 805
Koopmann, R. A., & Kenney, J. D. P. 1998, ApJ, 497, L75
Koopmann, R. A., & Kenney, J. D. P. 2004, ApJ, 613, 851
Koopmann, R. A., Haynes, M. P., & Catinella, B. 2006, AJ, 131, 716
Laine, S., Shlosman, I., Knapen, J. H., & Peletier, R. F. 2002, ApJ, 567, 97
Laurikainen, E., Salo, H., & Buta, R. 2004, ApJ, 607, 103
Martinet, L., & Friedli, D. 1997, A&A, 323, 363
Martini, P., Regan, M. W., Mulchaey, J. S., & Pogge, R. W. 2003, ApJ, 589, 774
Mestel, L. 1963, MNRAS, 126, 553
Muñoz-Mateos, J. C., Gil de Paz, A., Boissier, S., et al. 2007, ApJ, 658, 1006
Mulchaey, J. S., & Regan, M. W. 1997, ApJ, 482, L135
Petrosian, V. 1976, ApJ, 209, 1
Pompea, S. M., & Rieke, G. H. 1990, ApJ, 356, 416
Puxley, P. J., Hawarden, T. G., & Mountain, C. M. 1988, MNRAS, 231, 465
Roussel, H., Sauvage, M., Vigroux, L., et al. 2001, A&A, 372, 406
Ryder, S. D., & Dopita, M. A. 1994, ApJ, 430, 142
Sakamoto, K., Okumura, S. K., Ishizuki, S., & Scoville, N. Z. 1999, ApJ, 525, 691
Seigar, M. S., & James, P. A. 2002, MNRAS, 337, 1113
Sheth, K., Vogel, S. N., Regan, M. W., et al. 2002, AJ, 124, 2581
Sheth, K., Vogel, S. N., Regan, M. W., Thornley, M. D., & Teuben, P. J. 2005, ApJ, 632, 217
Shimasaku, K., Fukugita, M., Doi, M., et al. 2001, AJ, 122, 1238
Shlosman, I., Frank, J., & Begelman, M. C. 1989, Nature, 338, 45
Shlosman, I., Begelman, M. C., & Frank, J. 1990, Nature, 345, 679
Shlosman, I., Peletier, R. F., & Knapen, J. H. 2000, ApJ, 535, L83
Somerville, R. S., Primack, J. R., & Faber, S. M. 2001, MNRAS, 320, 504
Tinsley, B. M., & Danly, L. 1980, ApJ, 242, 435
Tomita, A., Tomita, Y., & Saito, M. 1996, PASJ, 48, 285
Trujillo, I., & Pohlen, M. 2005, ApJ, 630, L17
Verley, S., Combes, F., Verdes-Montenegro, L., Bergond, G., & Leon, S. 2007, A&A, 474, 43
Wada, K. 2004, in Coevolution of Black Holes and Galaxies, ed. L. C. Ho, 186
Wada, K., & Habe, A. 1995, MNRAS, 277, 433